The effect of bond-line thickness on fatigue crack growth rate in adhesively bonded joints

Pascoe, J. A.; Zavatta, N.; Troiani, E.; Alderliesten, R. C.

DOI
10.1016/j.engfracmech.2020.106959

Publication date
2020

Document Version
Final published version

Published in
Engineering Fracture Mechanics

Engineering Fracture Mechanics 229 (2020) 106959

Contents lists available at ScienceDirect

Engineering Fracture Mechanics

journal homepage: www.elsevier.com/locate/engfracmech

The effect of bond-line thickness on fatigue crack growth rate in adhesively bonded joints

J.A. Pascoe[a], N. Zavatta[b,*], E. Troiani[b], R.C. Alderliesten[a]

[a] Structural Integrity & Composites Group, Faculty of Aerospace Engineering, Delft University of Technology, Kluyverweg 1, 2629 HS Delft, the Netherlands

[b] MaSTeR Lab, Department of Industrial Engineering, University of Bologna, via Fontanelle 40, 47121 Forlì, FC, Italy

ARTICLE INFO

Keywords:
Fatigue crack growth
Adhesive bonding
Strain energy
Plasticity
Thickness effect

ABSTRACT

The effect of adhesive thickness on fatigue crack growth in an epoxy film adhesive (FM94) was investigated, using a combination of experiments and numerical modelling. For the range of thicknesses investigated an increased thickness led to an increased crack growth rate. It was found that the energy required per unit of crack growth did not depend on the adhesive thickness. In contrast, the energy available for crack growth does depend on the adhesive thickness.

The numerical analysis confirms that the energy required per unit crack growth is not sensitive to the adhesive thickness, but that the plastic energy dissipation increases with the thickness. The experimental results imply that this increase of plasticity has an anti-shielding effect, as the crack growth rate is increased.

1. Introduction

Compared to mechanical fastening, adhesive bonding offers the promise of lower weight structural joints. This is achieved by creating a smoother load transfer and removing the need for holes, and thus stress concentrations. Consequently adhesive bonding is an attractive option for structural designs in mass-critical applications, such as aerospace and automotive.

Before adhesive bonding can be applied on a wide scale however, more understanding is needed of its fatigue crack growth (FCG) behaviour. Many prediction methods have been proposed in the past, but these are all based on empirical correlations rather than an understanding of the physics [1]. Pascoe et al. [2,3] and Alderliesten [4] have suggested that more insight into the underlying physics can be gained by measuring the dissipation of strain energy during the crack growth process. They showed that correlating the crack growth rate to the measured strain energy dissipation per cycle (dU/dN), rather than to the strain energy release rate (SERR), could account for most of the effect of the stress ratio (R).

A small stress ratio effect was still observed. It was suggested that this might be caused by non-linearity of the force-displacement curve [3]. However further examination has shown that the force-displacement curve remains linear throughout the fatigue test [5]. An alternative hypothesis is that the observed difference in energy dissipation at different stress ratios, for a given crack growth rate, is caused by differences in the stress state and amount of plasticity at the crack tip. It is known from previous work that adhesive thickness affects these parameters [6–10], and thereby the fracture toughness.

While various studies on the effect of layer thickness on fatigue crack growth have been published [11–20], identifying that thickness can have an effect, the reported results are not consistent. Furthermore there has been little effort to understand the mechanisms that cause adhesive thickness to affect the fatigue crack growth rate.

* Corresponding author.
E-mail address: nicola.zavatta2@unibo.it (N. Zavatta).

https://doi.org/10.1016/j.engfracmech.2020.106959
Received 13 December 2019; Received in revised form 4 February 2020; Accepted 23 February 2020
Available online 10 March 2020
0013-7944/

Nomenclature

a	crack length [mm]
A	crack area [mm^2]
C	compliance [mm/N]
d	displacement [mm]
d_0	displacement for zero force [mm]
G	strain energy release rate [mJ/mm^2]
G^*	energy dissipation per unit of crack growth [mJ/mm^2]
n	Compliance Calibration parameter
N	number of cycles
P	force [N]
R	stress ratio
R_d	displacement ratio
R_p	force ratio
t	thickness [mm]
U	strain energy [mJ]
U_{pl}	plastic energy dissipation [mJ]
V_{adh}	volume of the adhesive [mm^3]
w	specimen width [mm]

Greek symbols

ε_{pl}	plastic strain tensor
σ	stress tensor [MPa]

Subscripts

c	critical
cyc	cyclic
m	optimum
max	maximum
min	minimum

Thus the present work examines the effect of different bond-line thicknesses on the FCG behaviour in FM-94 epoxy adhesive, as a way of gaining more understanding of the effect of the crack-tip plastic zone on crack growth behaviour. This is done by comparing results from crack growth experiments on double cantilever beam (DCB) specimens with different adhesive thicknesses with numerical modelling to determine the amount of plasticity. Before presenting the results of this research, the existing literature on the effect of adhesive thickness on crack growth will be discussed.

2. Literature review on the effect of adhesive thickness

Several studies on the effect of adhesive layer thickness on FCG rate are available in the literature [11–20]. A concise review of the effect of thickness on fracture (under quasi-static load) has been provided by Azari et al. [11].

In general, these works report that higher thickness results in lower FCG rates and also higher fracture toughness [11–13,15–17,19], which is ascribed to the effect of constraint (provided by the adherends) on the plastic zone size in the adhesive layer. Removal of constraint (by increasing thickness) is thought to result in more plasticity, which then increases the crack resistance, thus reducing the fatigue crack growth.

In contrast, Krenk et al. [14] reported no effect of thickness in a single-lap joint with a two-part cold-cured epoxy (9323, manufactured by 3M). Schmueser [18] found an increase of FCG rate for increasing adhesive thickness in a cracked-lap-shear (CLS) specimen, with a one-part epoxy (Ciba-Geigy Araldite XB-3131). In this case it should be noted that the loading mode-mix was different for the different adhesive thicknesses.

Chai [13] investigated two brittle epoxies (Namco 5208 and Hercules 3502) and one tough resin (PEEK) and found different behaviours. For the brittle epoxies the fracture toughness increased for increasing thickness. For PEEK, however, at low thicknesses ($t < 0.038$ mm) the fracture toughness first decreased with increasing thicknesses, and only at higher thicknesses did the toughness increase with increasing thickness.

Wilson [20] investigated delamination in Glare fibre metal laminates, which consist of aluminium and glass-fibre reinforced epoxy layers. By adding extra layers of unreinforced epoxy Wilson changed the thickness of the adhesive layer between the glass-fibre reinforced epoxy and the metal. He found that increasing the adhesive thickness resulted in an asymptotic reduction of the delamination growth rate. Wilson suggested that this effect was caused by a shift in the failure locus from the metal/reinforced epoxy interface to the reinforced/unreinforced epoxy interface. It should be noted that in Wilson's work the crack growth in the epoxy was in mode II, whereas the present research only studied mode I.

Detailed studies explaining how bond line thickness affects fracture have been mainly confined to quasi-static loading. Nevertheless, these studies may also shed light on the fatigue behaviour. Kinloch and Shaw [6] identified that the effect on fracture toughness is non-monotonic. Up to an optimum thickness t_m the fracture toughness (G_c) increased with increasing thickness. Above t_m, an increase of the adhesive thickness resulted in a reduction of the fracture toughness.

Kinloch and Shaw explained this behaviour with the work of Bascom et al. [7] and Wang et al. [8], who studied the plastic zone and the stress fields ahead of the crack tip. Based on those works, Kinloch and Shaw [6] argue that for $t < t_m$ the adherends restrict the full development of the plastic zone. This reduces the adhesive's capacity to dissipate energy by mechanisms other than fracture, resulting in a lower fracture toughness. The lower t, the greater the restrictive effect of the adherends, and therefore the lower the fracture toughness will be.

For $t > t_m$, the dominant effect according to Kinloch and Shaw is the amount of constraint in the adhesive. As the thickness increases, the degree of constraint reduces. The reduction in constraint causes the plastic zone to extend less far ahead of the crack tip. This reduces the volume of the plastic zone, resulting in a reduction of fracture toughness.

These constraint effects were further investigated by Daghyani et al. [9], eventually leading Yan et al. [10] to propose a model

involving two different mechanisms. Yan et al. propose that a reduction in thickness increases the constraint on the adhesive, resulting in a reduction of the plastic zone size, and therefore a decrease of the fracture toughness. This is the primary mechanism when $t < t_m$. When the thickness is greater than the optimum thickness, an increase in thickness will allow increased crack tip blunting to occur, resulting in increased void-crack coalescence, and therefore a lower fracture toughness.

In contrast to the findings of Kinloch and Shaw, and Yan et al., a recent study by Azari et al. [21] found no evidence of an optimum thickness, reporting a linear increase of the toughness with adhesive thickness for all the tested thicknesses. This suggests that the Kinloch-Shaw and Yan et al. models may be material dependant. It is also possible that for the adhesive tested by Azari et al. the optimum thickness is larger than the maximum value investigated.

Pardoen et al. [22] investigated the effect of thickness based on a work of fracture approach. Their findings were in line with the Kinloch-Shaw and Yan et al. models, but did highlight a number of important considerations. First of all, Pardoen et al. performed a fractographic investigation, which identified that the fracture mechanisms (for the adhesive they investigated) take place on a length scale on the order of 100–200 μm. This means that at low adhesive thicknesses, not only the plastic zone, but also the fracture mechanisms themselves may be constrained by the adherents. Furthermore, Pardoen et al. pointed out that the intrinsic work of fracture of the adhesive, which is not affected by the plasticity, may itself also depend on the local stress state, and thereby on the adhesive thickness.

The works mentioned above all quantified the effect of thickness on the fracture toughness, i.e. the resistance to crack growth. However, the adhesive thickness might also affect the driving force for crack growth. That is, for the same applied far-field loading, a different thickness might result in a different driving force. Chiu and Jones [23] investigated the case of an undamaged bond, and found that the adhesive thickness affected the stress distribution. Gleich et al. [24,25] and Lenwari et al. [26] looked specifically at the stress intensity factor (SIF) at the bi-material interface at the end of the bond-line and found that the SIF increased for increasing adhesive thickness. It is unclear whether these results also hold for a cohesive crack within the adhesive layer. Nevertheless, they could help explain the apparent decrease of fracture toughness for increasing adhesive thickness reported in the papers mentioned above. After all, the fracture toughness there was measured based on the applied load. So, an increase in crack driving force for the same applied load would produce the impression of a lowered fracture toughness.

From the available studies one can conclude that in general, up to a certain optimum, a greater adhesive thickness will produce more plastic deformation, and as a result lower crack growth rates. The precise effects will however depend on the adhesive and geometry under consideration.

3. Specimens

For this research DCB specimens consisting of two Al2024-T3 arms bonded with FM94K.03AD epoxy film adhesive were used. This adhesive comes in the form of a film supported by a polyester carrier mat, i.e. a loose fibre weave, which allows for better control of the thickness. Three types of specimens, with different (nominal) adhesive thicknesses were investigated.

As a baseline, fatigue crack growth data from specimens containing a single layer of adhesive film were used. This data had been collected and published previously [5,27]. In the online datasets [5] these are referred to as series B through E. In this paper they will collectively be denoted as the 1l specimens, as they contained 1 layer of adhesive.

Two further types of specimens were manufactured specifically for this research. One type contained two layers of adhesive film

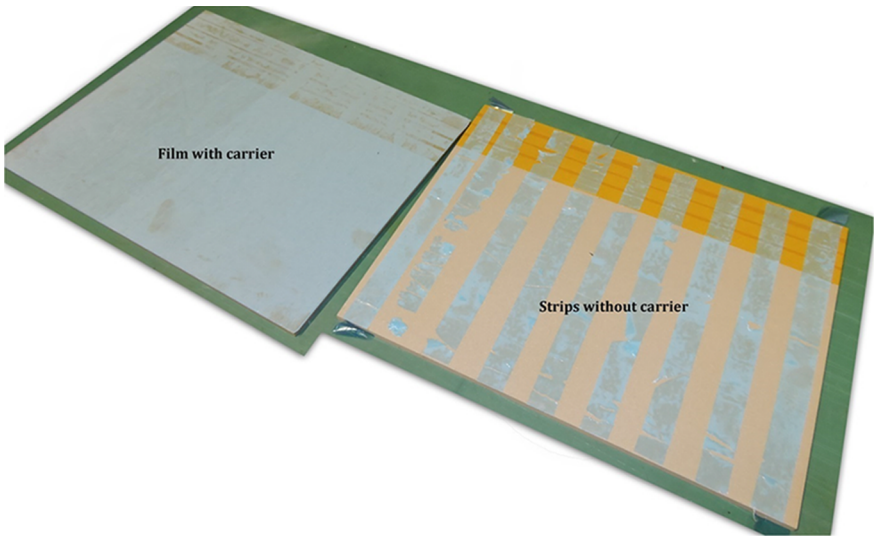

Fig. 1. Manufacturing of 1.5l specimens. The plate on the left is entirely covered by a sheet of epoxy film, the plate on the right is covered with strips of adhesive over approximately half of its surface area. The plates are then placed on top of each other, with the adhesive in the middle of the resulting stack [27].

(both with polyester carrier), and were denoted series G. This paper will collectively refer to them as the 2l specimens. The third type of specimens contained approximately 1.5 layers of adhesive film and are referred to as series H. This paper will collectively refer to them as the 1.5l specimens. Having '1.5 layers' of adhesive film was achieved during manufacturing by making an adhesive layer consisting of one layer of FM94K.03AD adhesive with carrier, and then placing strips of FM94-U-06 adhesive film without carrier on top of this, over approximately half the surface area. This is shown in Fig. 1. During curing the epoxy without carrier will flow, resulting in an adhesive layer thickness in between that of the single and the double layer specimens.

Of course, precise thickness control cannot be achieved with this manufacturing strategy. However, given that the adhesive thickness of each 1.5l and 2l specimen would be measured before testing, the expected thickness variation was considered acceptable. Another concern with this manufacturing strategy is that the different adhesive layers will not bond. However, based on prior experience and the observation (through measuring the adhesive thickness on both sides of the produced specimens) that the FM94-U-06 strips had indeed flowed enough during the bonding process to produce a uniform thickness layer, there is no reason to expect the layers did not bond.

The presence of a second carrier mat in the 2l specimens might also be expected to influence the results. Under quasi-static loading, the presence of fibres in the adhesive can result in fibre bridging and increase the toughness [28], so similar behaviour might be expected in fatigue. Nevertheless, previous research found that for mode I fatigue crack growth in an FM94 adhesive bond, the effect of a single carrier mat is negligible [29]. In the present research no results were found that suggested that the second mat had an influence but, considering the wide-spread use of carrier mats to control bondline thickness, more investigation of their effect in future research would be desirable.

The specimens were manufactured by bonding two plates of aluminium together for each specimen type. The aluminium plates had been pre-treated by chromic acid anodisation and application of BR-127 primer. A lay-up was created of the two plates, with the uncured epoxy film in between. This stack was then placed in a vacuum bag and cured in an autoclave according to the manufacturer's specifications (120°C for 1 h at 6 bar (0.6 MPa) with a 2°C/min heating and cooling rate). After curing, the plates were cut into strips, which were then milled down to a nominal width of 25 mm. Each of the aluminium arms had a nominal thickness of 6 mm (so a nominal total thickness of 12 mm + the adhesive thickness). The 1l specimens were 300 mm long and the 1.5l and 2l specimens were 270 mm long (in both cases based on the available adherend stock). As for all tests the crack never got closer than 100 mm to the end of the specimen, the difference in specimen lengths should not have any effect. The measured final dimensions of each specimen can be found in the online datasets [5,30].

Polyester adhesive tape was placed over a portion of the aluminium plates before bonding, in order to provide a pre-crack length of 50 mm (as measured from the load application points).

For the single layer specimens (1l), the bond line thickness was 0.07 mm [27]. The adhesive thickness as measured at the mid-point of the specimen length for the 1.5l specimens and the 2l specimens is reported in Table 1.

Compared to most of the literature (with the exception of Chai [13] and Wilson [20], and to a certain extent also Azari et al. [11] and Mall and Ramamurthy [16]), this research focussed on lower thicknesses (maximum thickness on the order of 0.3 mm).

Since in most cases multiple fatigue tests were conducted on the same specimen, the tests were labelled with the scheme: [letter]-[number]-[Roman numeral], where the letter refers to the specimen series, the number to the specimen number in that series, and the Roman numeral refers to the number of the test on that specimen. So, e.g. E-003-II refers to the second test conducted on specimen 003 in series E. Due to issues with the test set-up (e.g. in one case the loading block became detached from the fatigue machine), not all tests produced valid crack growth data. Only the tests that produced valid data have been included in this paper.

4. Test set-up

Fatigue tests were performed on an MTS 10 kN fatigue testing machine at 5 Hz under displacement control. Force and

Table 1
Adhesive thickness at the mid-point of the specimen, measured using an optical microscope aimed at the side of the specimen. As the 1 adhesive layer specimen data were taken from an earlier research project, adhesive layer thickness measurements were not available for each specimen individually.

Type	Specimen ID	Thickness [mm]
1 layer	Average	0.07
1.5 layers	H-002	0.195 ± 0.005
	H-003	0.135 ± 0.005
	H-004	0.245 ± 0.015
	H-006	0.220 ± 0.010
	H-008	0.210 ± 0.010
2 layers	G-002	0.275 ± 0.015
	G-006	0.275 ± 0.005
	G-008	0.275 ± 0.005
	G-009	0.265 ± 0.015
	G-010	0.285 ± 0.005

displacement were measured by the fatigue bench and crack lengths were measured using a camera aimed at the side of the specimen. The resolution of image used to determine the crack length was approximately 20 pixels/mm. An extended discussion of the test set-up has been published by Zavatta [31].

The specimens were connected to the fatigue machine using loading blocks that were attached to the specimen by bolts, as shown in Fig. 2.

Prior to each fatigue test, the specimens were quasi-statically loaded in displacement control, until crack propagation was observed visually. This ensured that the specimens contained a 'fresh' cohesive pre-crack in the adhesive layer. Even though the crack starters were placed at the adhesive/adherent interface, the quasi-static loading caused the crack to jump into the bulk of the adhesive layer. This was also verified by post-mortem inspection of the fracture surfaces of a number of the specimens.

As mentioned above, the 1l results were collected during a previous test programme [27]. Initially tests were conducted to obtain certain ratios of $\Delta G/G_{max}$ (series B and C [5]). This resulted in 4 different force-ratios ($R_p = P_{min}/P_{max}$): 0.036; 0.29; 0.61 and 0.86. To be able to compare that data with the data collected in subsequent tests, follow up tests on the 1l specimens were performed using these 4 values as the displacement ratio $R_d = d_{min}/d_{max}$. These displacement ratios were also used for the 1.5l and 2l tests. As the force-displacement curve did not pass exactly through the origin, the force ratios were not exactly equal to the displacement ratios. The obtained force ratios are shown in Table 2, which shows an overview of all experiments discussed in this paper. For clarity of presentation the tests have been grouped according to the 4 target R-ratios.

For $R_p = 0.86$ the amount of crack growth produced for the 1.5l and 2l specimens was too small to be able to take accurate measurements, so the results for those experiments will not be discussed further here.

5. Data analysis

The crack growth rate was determined by fitting a power-law equation through the a vs N data and then taking the derivative. The SERR was computed using the compliance calibration (CC) method [32], i.e.:

$$G = \frac{nPd}{2wa} \tag{1}$$

where P is the force, d is the displacement, w is the specimen width, a is the crack length, and n is a calibration parameter that is determined from the slope of a linear fit through log C vs log a, where C is the specimen compliance. In this research, n was determined for each experiment individually.

The energy dissipation per cycle dU/dN was computed by taking the derivative of a power-law fit through the total strain energy, U, vs N data, following the method presented previously by Pascoe et al. [3]. U was computed as:

$$U = \frac{1}{2}P_{max}(d_{max} - d_0) \tag{2}$$

where d_0 is the displacement for which the recorded force was zero.

The raw and processed data used in this paper are available online [5,30,33].

6. Experimental results

When following the traditional method of plotting crack growth rate against maximum SERR, the results shown in Fig. 3 are

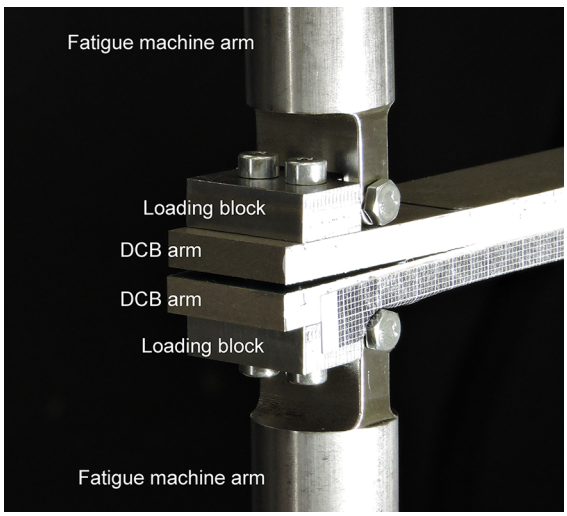

Fig. 2. Loading blocks used to connect the specimens to the fatigue machine.

Table 2
Achieved force and displacement ratios as determined post-test. The grouping of the tests by R-ratio is also shown.

Type	Experiment	R_d	R_p	Group
1 layer	B-001-II	0.1	0.036	0.036
	B-002-I	0.88	0.86	0.86
	B-002-II	0.74	0.61	0.61
	C-001-I	0.33	0.29	0.29
	C-002-D	0.67	0.61	0.61
	D-002-I	0.29	0.29	0.29
	E-001-I	0.29	0.24	0.29
	E-001-II	0.29	0.27	0.29
	E-002-I	$2.3{\cdot}10^{-4}$	−0.022	0.036
	E-002-II	$-9.3{\cdot}10^{-5}$	0.014	0.036
	E-003-I	0.61	0.60	0.61
	E-003-II	0.61	0.62	0.61
1.5 layers	H-002-I	0.036	0.0054	0.036
	H-002-II	0.033	−0.0070	0.036
	H-003-I	0.29	0.24	0.29
	H-003-II	0.29	0.25	0.29
	H-004-I	0.61	0.56	0.61
	H-006-I	0.61	0.56	0.61
	H-008-I	0.86	0.83	0.86
2 layers	G-002-I	0.29	0.25	0.29
	G-002-II	0.29	0.23	0.29
	G-006-III	0.036	$-3.1{\cdot}10^{-4}$	0.036
	G-008-I	0.61	0.47	0.61
	G-009-I	0.61	0.56	0.61
	G-010-I	0.86	0.83	0.86
	G-010-II	0.033	−0.039	0.036

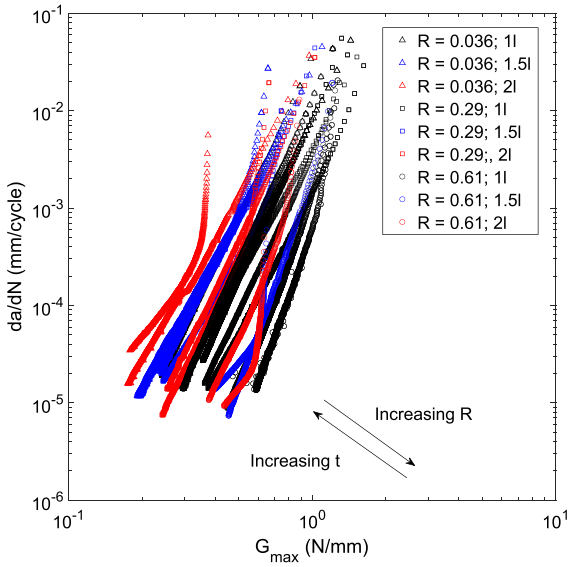

Fig. 3. Crack growth rate as a function of maximum SERR. The results are grouped by number of adhesive layers: 1 layer (1l), '1.5 layers' (1.5l) and 2 layers (2l), and R-ratio, with at least 2 experiments per combination of R-ratio and number of layers. Higher R-ratio results in slower crack growth, while higher adhesive thickness results in faster crack growth.

obtained. As expected there is an R-ratio effect: higher R-ratios mean a lower crack growth rate. This is to be expected, as a higher R-ratio means a lower ΔG.

The effect of the adhesive thickness can be more clearly seen in Figs. 4 and 5. Fig. 4 shows the $\mathrm{d}a/\mathrm{d}N$ vs $G_{\max}$ data, grouped per R-ratio. Fig. 5 shows for each experiment the $G_{\max}$ that resulted in a crack growth rate of 10^{-4} mm/cycle, as a function of bond-line thickness. In Fig. 5, linear fits through the data are shown, one for each R-ratio, as a guide to the eye. However, given what is known about the effect of thickness, it is likely that the actual dependence of $G_{\max}$ on t for a given $\mathrm{d}a/\mathrm{d}N$ is non-linear.

There is a clear effect of adhesive thickness: increasing the thickness from one layer caused an increase in crack growth rate for the same load cycle. The effect of increasing from 1 layer to 1.5 layers appears to be larger than that of increasing from 1.5 layers to 2

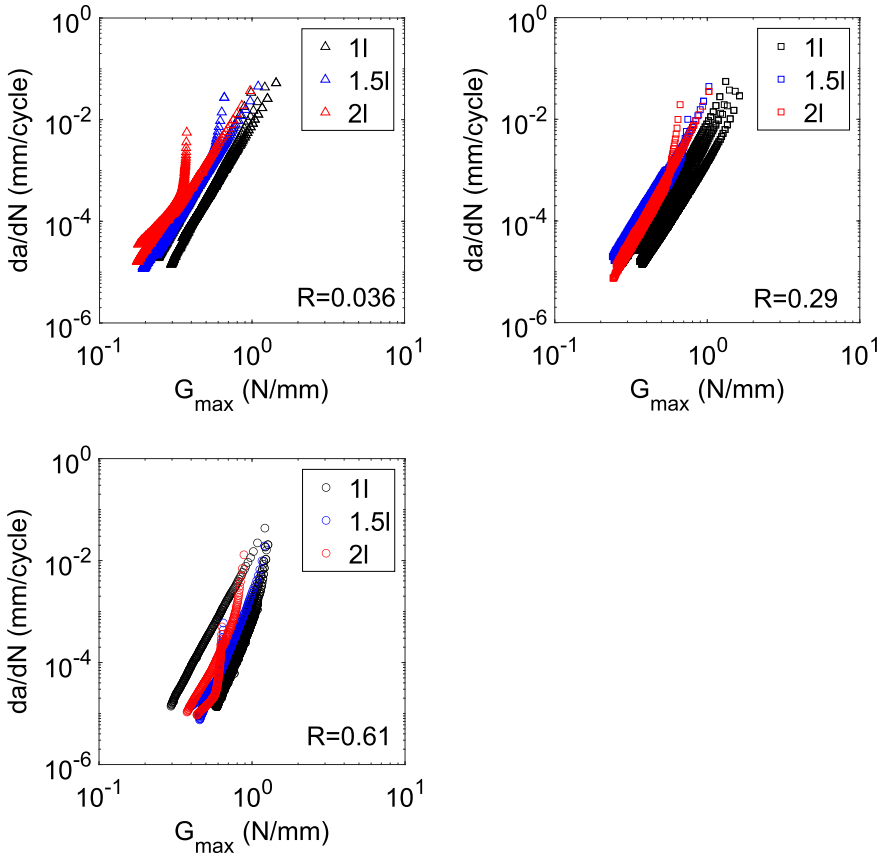

Fig. 4. Crack growth rate as a function of maximum SERR. The results are displayed for each R-ratio individually, in order to better see the effect of thickness.

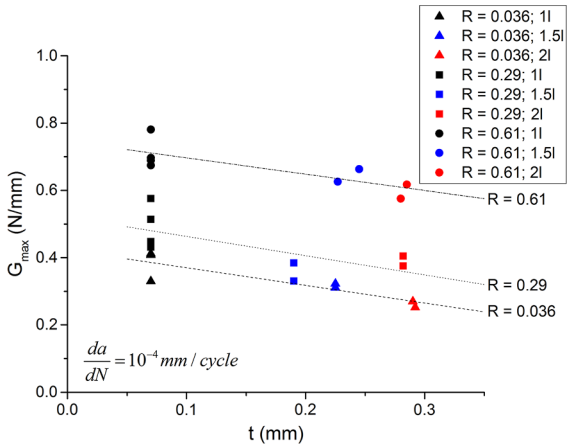

Fig. 5. G_{max} required for a crack growth rate of 10^{-4} mm/cycle as a function of adhesive thickness. Each point corresponds to one experiment. Linear fits of G_{max} vs t for each R-ratio are shown as guides-to-the-eye.

layers. However, it should be noted (as can be seen in Table 1 and Fig. 5) that going from 1 to 1.5 layers also caused a larger increase of the final bond-line thickness than going from 1.5 to 2 layers.

In contrast to the traditional method, Fig. 6 shows the crack growth rate plotted against the strain energy dissipation per cycle dU/dN. Here the data fall into a narrow band, except for three experiments: G-006-III (2 layers, $R = 0.036$), H-006-I (1.5 layers, $R = 0.61$) and G-008-I (2 layers, $R = 0.61$).

For H-006-I and G-008-I these anomalous relationships can potentially be explained by the observed crack growth behaviour. In these experiments secondary cracks growing along the adhesive/adherent interface were observed. Fig. 7 shows a photograph of the

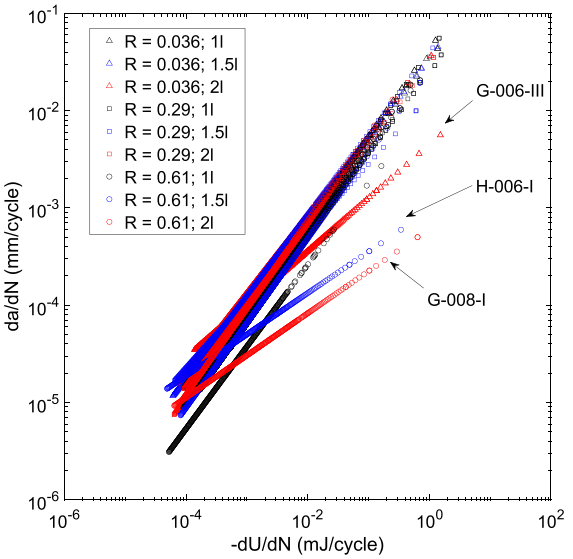

Fig. 6. Crack growth as a function of energy dissipation per cycle. There are three clear outliers. For experiments H-006-I and G-008-I the anomalous behaviour is thought to be caused by the formation of secondary cracks along the adhesive/adherent interface. For G-006-III the cause is unclear. For all three outliers, repeated experiments under the same conditions do match the other experiments.

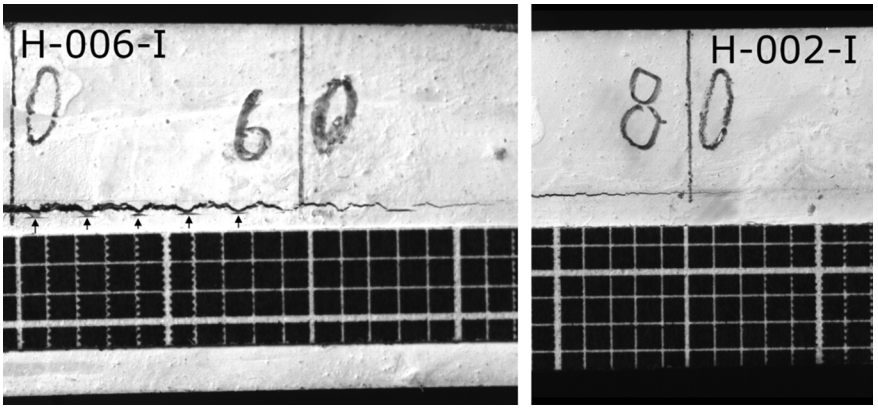

Fig. 7. Comparison between a test where secondary interface crack growth was seen (H-006-I, left) and typical crack growth (H-002-I, right). The location of the secondary cracks is marked by the arrows. These cracks are thought to be the reason for the increased energy dissipation per unit of crack growth for experiments H-006-I and G-008-I [27].

secondary cracks, and Fig. 8 shows schematically the definition of secondary crack. These secondary cracks were not present during the other experiments, but have also been noted in other experimental studies [34]. The growth of these secondary cracks will also dissipate energy, while not producing an advance of the main crack tip. As a consequence, the total amount of energy dissipated per unit of growth of the main crack will be increased, which is what is seen in Fig. 6. Goutianos and Sørensen [35] have also shown analytically that secondary cracks will increase the fracture toughness. The reason for secondary crack growth to occur in this case is unclear.

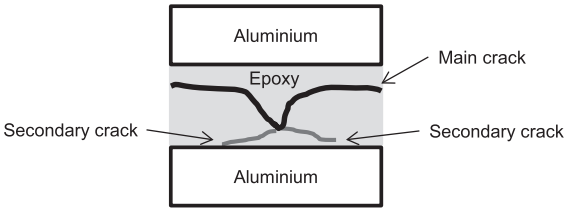

Fig. 8. Schematic illustration showing the definition of secondary cracks, as referred to in Fig. 7.

Furthermore, no secondary cracks were observed for experiment G-006-III, and therefore the reason for the anomalous behaviour during this experiment remains unclear. Note that for all three of these anomalous experiments a second experiment was conducted under the same load conditions. During these repeat experiments no secondary crack growth was observed, and the data for these repeat experiments falls into the same band as for the bulk of the experiments.

To more clearly see the effect of thickness, Fig. 9 shows the data of Fig. 6 but now separated into different plots; one for each R-ratio. Figs. 6 and 9 show that the effect of adhesive thickness on the relationship between energy dissipation and crack growth rate is limited, especially in comparison to the effect of thickness on the relationship between crack growth rate and G_{max}.

Fig. 10 shows the fracture surfaces for 4 experiments, all performed at $R = 0.61$. In each case the fracture surface at the end of the fatigue crack is shown, and a small amount of quasi-static fracture is also visible. This was caused by the quasi-static loading used to break apart the specimens. The crack grew from left to right. The dark areas indicate fatigue crack growth and the light areas indicate quasi-static crack growth. Imprints left by the fibres of the carrier mat can also be seen, in the form of a diamond-shaped pattern. No obvious differences could be found between the different adhesive thicknesses. There are also no obvious differences between the experiments that were outliers in Figs. 6 and 9 (G-008-I, bottom left, and H-006-I, top right) and the experiments that showed 'normal' behaviour (E-003-II, top-left, and G-009-I, bottom-right).

Another way of examining this is by looking at the amount of energy dissipated per unit of crack growth, G^*, which was calculated from the experimental data according to:

$$G^* = \frac{1}{w}\frac{\mathrm{d}U/\mathrm{d}N}{\mathrm{d}a/\mathrm{d}N} \tag{3}$$

Eq. (3) reduces to $G^* = \frac{1}{w}\frac{\mathrm{d}U}{\mathrm{d}a}$, which is equal to the expression for the SERR. However, it should be noted that the SERR as defined by Irwin [36,37] is a proper derivative in the mathematical sense, whereas G^* is an average over one fatigue cycle.

As G^* represents the amount of energy dissipated per unit of crack growth, it can be seen as a measure of the crack growth resistance. More energy dissipation per unit of crack growth means it is harder for the crack to grow. Thus G^* can be used to investigate whether the crack resistance is constant or not. It should be noted however, that G^* measures all forms of energy dissipation. Therefore it can only be used to say something about the crack resistance if there are no other dissipative mechanisms active that are unrelated to crack growth.

In Fig. 11 G^* is compared to the maximum SERR value G_{max}. For most of the data there is a linear relationship between G^* and G_{max}. The exceptions are the three experiments that were identified as outliers in Fig. 6, as well as experiments B-001-II (1 layer,

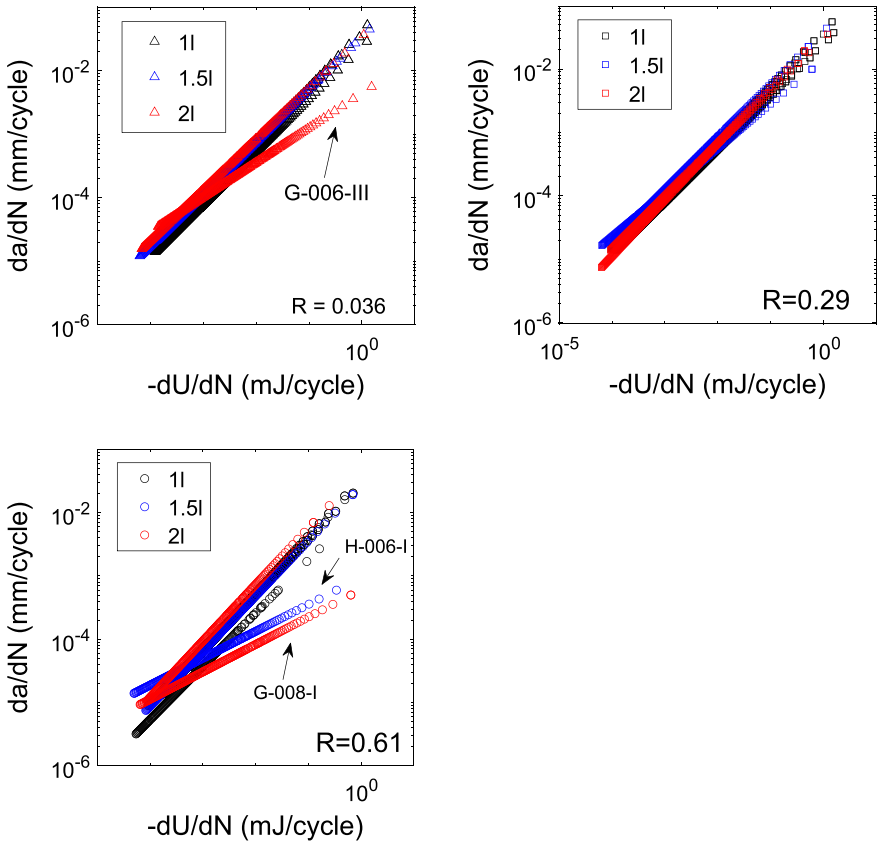

Fig. 9. Crack growth rate as a function of energy dissipation per cycle, grouped by R-ratio.

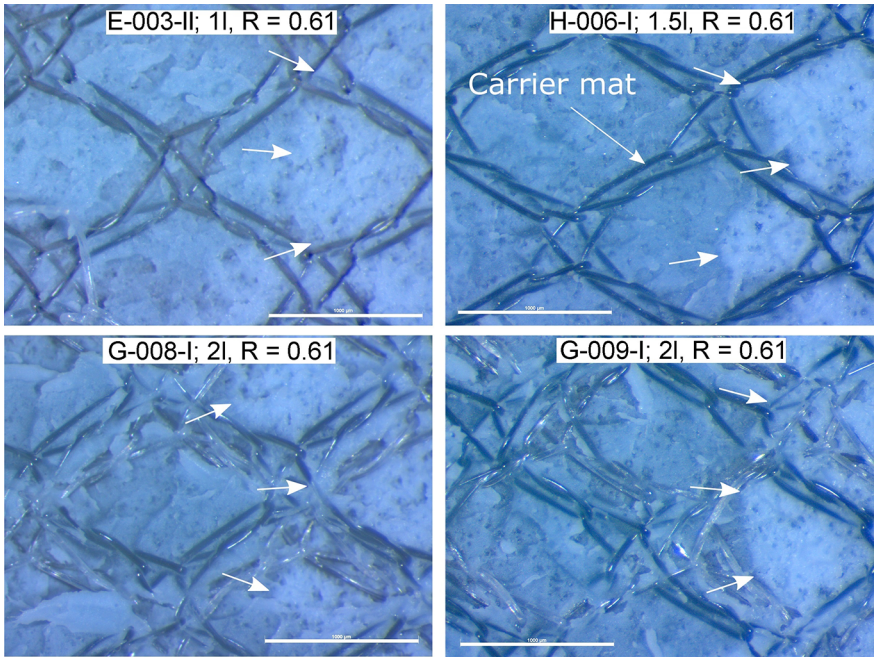

Fig. 10. Fracture surfaces from 4 different experiments. In each case the specimen was tested at $R = 0.61$, but the number of adhesive layers was different. In each case, the end of the fatigue test is shown (i.e. low $\mathrm{d}a/\mathrm{d}N$). Crack growth was from left to right. The white arrows indicate the front of the fatigue crack, i.e. the boundaries of the darker area. The fibres of the carrier mat and their imprints on the adhesive can also be seen. The scale bars in each picture indicate a length of 1 mm.

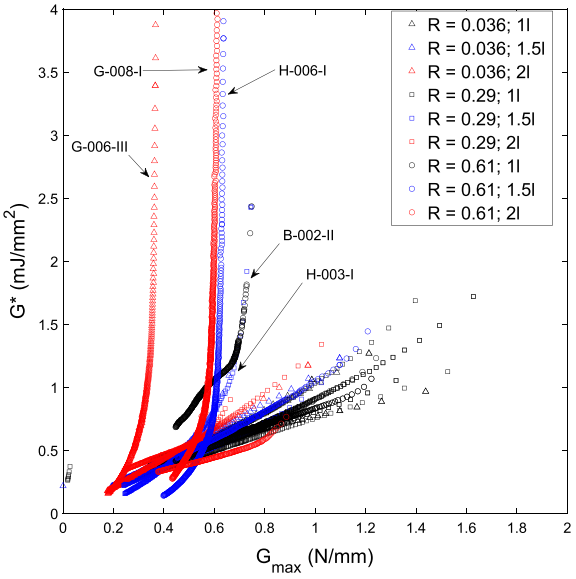

Fig. 11. Energy dissipation per unit of crack growth (G^*) as a function of maximum SERR.

$R = 0.61$) and H-003-I (1.5 layers, $R = 0.29$). For these experiments the G^* value rises asymptotically as G_{max} approaches a certain value. Apart from the outliers, the curves for the higher adhesive thickness specimens seem to follow the same linear trend as those for the single layer specimens, and even the asymptotic curves follow this trend at low G_{max} values.

For G-008-I (2 layers; $R = 0.61$) and H-006-I (1.5 layers; $R = 0.61$) the difference in behaviour compared to the other specimens seems to be linked to the secondary crack growth discussed above. In Fig. 7 it can be seen that the secondary crack growth was only seen during the early part of the test, when the G_{max} value is high. In the later part of the test (low G_{max}) the crack advanced without generating new secondary cracks. This can also be seen in Fig. 11: for low G_{max} values the G^* value matches that seen during the tests without secondary crack growth.

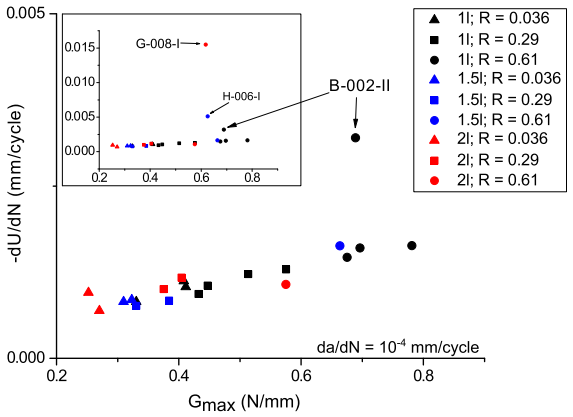

Fig. 12. Energy dissipation versus maximum SERR for a crack growth rate of 10^{-4} mm/cycle. The inset graph shows a zoomed-out view that also shows the data points for experiments G-008-I and H-006-I. G-008-I and H-006-I are again outliers due to the secondary crack growth. Each point corresponds to a different experiment.

Another view on the amount of energy required for crack growth is given by Fig. 12, which shows how much energy was dissipated for a crack growth of 10^{-4} mm/cycle, as a function of G_{max}. The figure shows that for a given R-ratio, for higher adhesive thickness, the amount of energy dissipated to produce 10^{-4} mm/cycle crack growth rate was lower. On the other hand, the relationship between the dissipated energy and G_{max} is unaffected by the adhesive thickness. This suggests that, in the present case, an increase of adhesive thickness has an anti-shielding effect. Increasing the thickness makes the crack growth process more efficient: less energy is required for the same amount of crack growth.

The previous figures relate to how much energy is required to produce a certain amount of crack growth. Thus it is also instructive to examine the amount of energy available for crack growth. By the first law of thermodynamics, the amount of energy available in a cycle must equal the amount of energy dissipated. It was noted elsewhere [27,38] that if G^* is fixed (i.e. the resistance to crack growth is the same), then the energy dissipation is strongly correlated to the applied cyclic work U_{cyc}, which is defined as:

$$U_{cyc} = \frac{1}{2}(P_{max}d_{max} - P_{min}d_{min}) \tag{4}$$

Fig. 13 shows the energy dissipation as a function of U_{cyc} for a fixed G^*. Although the correlation between dU/dN and U_{cyc} is not that strong, it is clear that for a given value of U_{cyc} the amount of energy dissipated in the increased thickness specimens is much higher than that dissipated in the single adhesive layer specimens.

Together Figs. 11 and 13 show that the amount of energy dissipated per unit of crack growth (G^*) depends on G_{max}, but does not seem to be affected by the adhesive thickness. However, an increase in adhesive thickness will result in a larger total amount of energy dissipation (dU/dN), implying more energy is available for crack growth. The net result is that for a given load cycle (i.e. combination of G_{max} and U_{cyc}), the energy dissipation required per unit crack growth is not affected by the thickness, but the total energy dissipation in the cycle is higher if the adhesive layer is thicker. As a result, the crack growth rate will be higher for higher adhesive thickness.

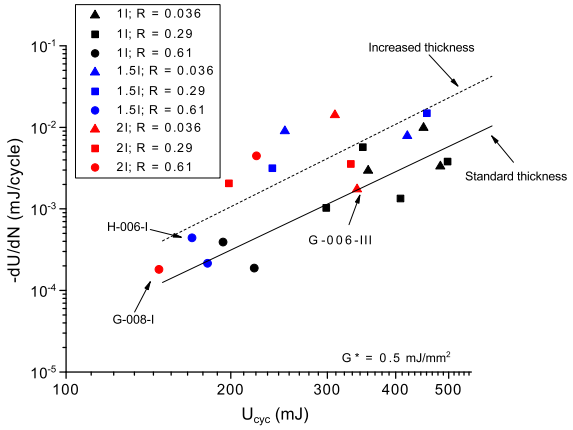

Fig. 13. Energy dissipation as a function of U_{cyc} for a fixed value of $G^* = 0.5$ mJ/mm^2. Power law fits are shown for the standard data, and the increased thickness data, as guides to the eye. Each point corresponds to a different test. The experiments previously identified as outliers have been indicated.

7. Numerical model and results

In order to evaluate the energetic contribution of the adhesive, a 2D finite element model under quasi-static loading was developed in the commercial software package *Abaqus*. The geometry of the model was equal to that of the tested specimens, i.e. a double cantilever beam with same dimensions. The adherends were modelled as aluminium plates, while the adhesive was modelled as an epoxy layer cut by the disbond surface along its midline. Three different configurations of the epoxy layer were considered, corresponding to 1 layer, 1.5 layers and 2 layers of adhesive, which resulted in an adhesive thickness equal to 0.08, 0.20 and 0.28 mm respectively. Ten simulations were run for each configuration, varying the disbonded area from a length of 55 mm to 100 mm.

Both the aluminium and the epoxy were modelled as isotropic materials with elastic-plastic behaviour; the elasto-plastic properties of Al2024-T3 and of the FM94 epoxy are reported in the literature [39–41]. The virtual crack closure technique (VCCT) [42,43] was used to compute the strain energy release rate in the adhesive. A similar application of the VCCT to yielding of FM-300 adhesive is discussed in Jokinen et al. [44].

The entire specimen was meshed with second-order plain strain elements with quadrangular shape, i.e. types CPE8 and CPE8R in Abaqus. A uniform mesh was used in the adhesive and the same element size was employed for all three configurations. This resulted in a total of 4, 10 and 14 elements through the adhesive thickness for the 1l, 1.5l and 2l cases respectively.

The model was loaded under displacement control similarly to the experimental tests. First a linear displacement equal to $d_{\max}$ was applied to the specimen, then it was unloaded down to a displacement of $d_{\min}$ and then loaded up again to $d_{\max}$. Globally, this reproduces the loading conditions occurring during a single cycle in the fatigue tests. The values $d_{\max} = 2.85$ mm and $d_{\min} = 1.89$ mm were used in the simulations, which are numerically equal to those applied to specimen C-002-D in the tests.

Fig. 14 shows a comparison of the strain energy release rate G computed by the VCCT in the three different configurations of adhesive thickness. The G calculated from experimental data on single layer specimens is also plotted for comparison. Only specimens with an applied displacement comparable to that used in the simulations are reported. The variation of strain energy release rate in the three configurations is as little as 7%. This suggests that, at least for the range of thicknesses considered here, varying the adhesive thickness has little effect on G.

The G computed by the VCCT differs by no more than 15% from the experimental results for all the considered disbond lengths. The numerical and experimental curves tend to diverge for short disbonds, which can be put down to the large scatter present in the experimental data for these points. Comparing the numerical results to the data from specimen C-002-D, which were obtained under basically the same cyclic displacement, shows an almost complete overlapping of the curves for both the maximum and minimum strain energy release rates, which suggests that both the upper and lower part of the loading cycle are well reproduced by the model.

No plasticity occurs in the aluminium adherends, in accordance to what was observed in the tested specimens. On the contrary, the yield strength of the epoxy is exceeded in a region around the crack tip, which extends all the way through the adhesive thickness, as shown in Fig. 15. This means that a plastic deformation is produced in the adhesive layer during the loading cycle, which is not recovered after unloading. As a result, a net amount of energy associated to the plastic strain is dissipated in the process. This plastic energy dissipation can be computed as:

$$U_{\text{pl}} = \int_{V_{\text{adh}}} \boldsymbol{\sigma} : \boldsymbol{\varepsilon}_{\text{pl}}\, dV \tag{5}$$

where V_{adh} is the volume of the adhesive, $\boldsymbol{\sigma}$ is the stress tensor and $\boldsymbol{\varepsilon}_{\text{pl}}$ the plastic strain tensor. The plastic dissipation per unit crack growth is given by $\frac{dU_{\text{pl}}}{dA} = \frac{1}{w}\frac{dU_{\text{pl}}}{da}$. The amount of plastic dissipation depends on the applied work, which in a single cycle is equal to U_{cyc}

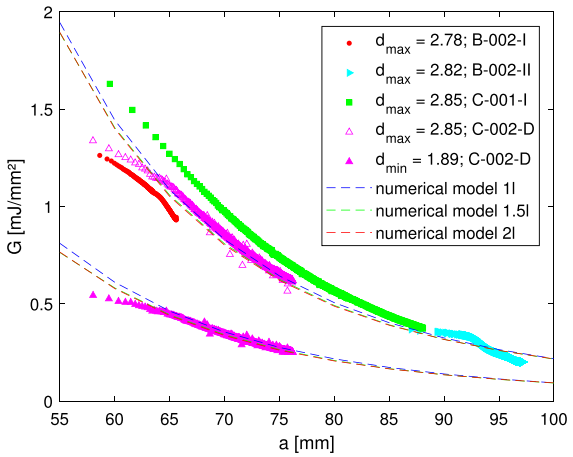

Fig. 14. Comparison of the strain energy release rate computed in the 1l, 1.5l and 2l configurations. The experimental results for the single layer specimen are also shown. The displacement applied in the simulations is equal to 2.85 mm for the upper dashed lines and to 1.89 mm for the lower ones. The bottom values of G for specimens other than C-002-D are not reported as the minimum displacement applied in those tests is different from that used in the numerical simulation.

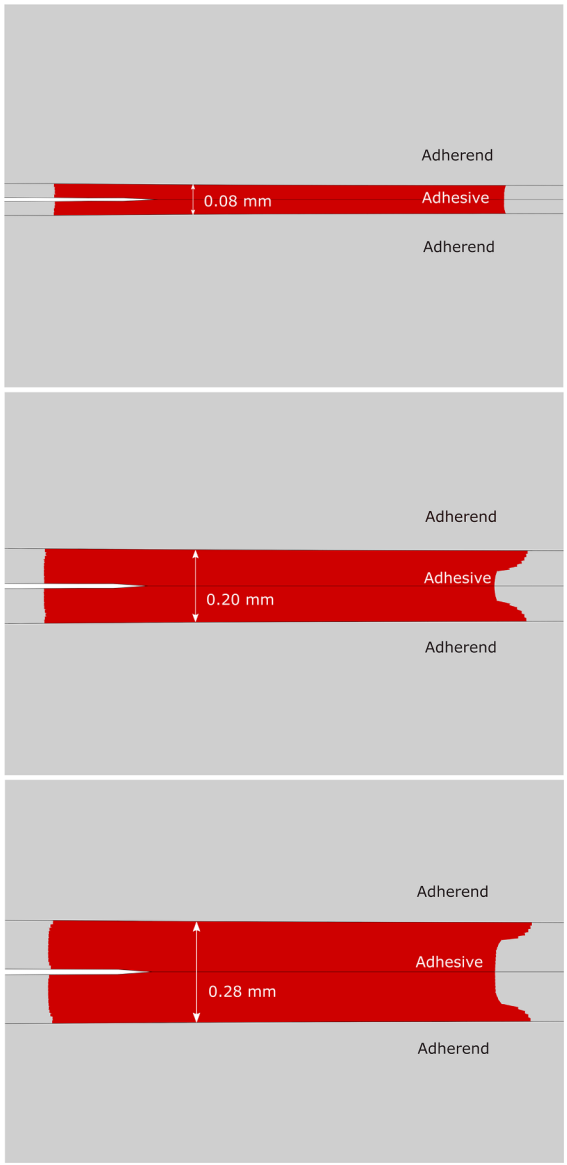

Fig. 15. Size of the plastic zone for different adhesive thicknesses: in red is shown the region where the plastic strain is non-zero, in grey the elastic regions. The same scale is used in the three cases.

and can be calculated according to Eq. (4).

The plastic energy dissipation is affected by the adhesive thickness, as shown in Fig. 16. The thicker the adhesive layer, the more energy is dissipated by plasticity for a given applied energy. The relationship between the amount of dissipated energy and the adhesive thickness is non-linear, as it is clearly visible from the figure: increasing the thickness from 0.08 mm (1l) to 0.20 mm (1.5l) results in a plastic dissipation which is 1.6 times the original value; an additional increase to 0.28 mm only increases the dissipation further of about 10%.

8. Discussion of experimental and numerical results

The experimental results show that the adhesive thickness has little effect on the energy dissipated per unit of crack surface created (Fig. 11). At the same time, the adhesive thickness does affect the total amount of energy dissipated, for a given load cycle (Fig. 13).

A comparison between Figs. 3 and 11 shows that despite the higher G^* for higher G_{max}, the crack growth rate is also higher. That is to say: although more energy is being dissipated per unit of crack growth, the crack growth rate is also higher. That faster crack growth requires more energy dissipation per unit of growth has been observed previously [45], though not to the extent seen here.

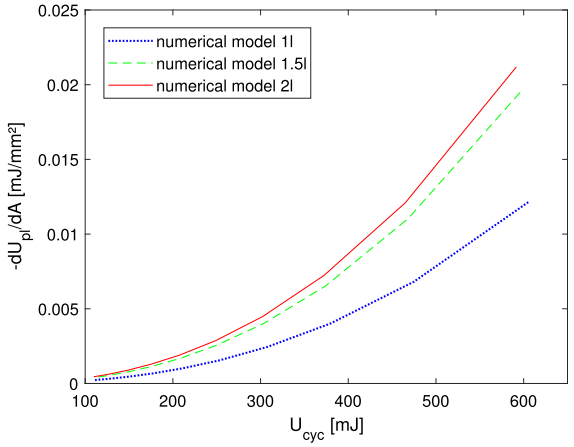

Fig. 16. Plastic energy dissipated per unit crack growth as a function of the applied cyclic energy.

This implies that increasing G_{max} not only increases the resistance (in terms of required energy per unit crack growth), but also the amount of energy available for crack growth.

In particular, it appears that the secondary crack growth seen during experiments G-008-I and H-006-I is able to make use of a 'reservoir' of energy that is not available for normal crack growth. Otherwise it cannot be explained that the same crack growth rate is achieved for much higher G^* values.

Although no secondary crack growth was seen for experiments G-006-III (2 layers; $R = 0.036$), B-001-II (1 layer; $R = 0.61$), and H-003-I (1.5 layers; $R = 0.29$), the similarity in the shape of the G^* vs G_{max} curves to those for G-008-I and H-006-I suggests that also for these specimens there is some form of dissipative mechanism that is activated at high G_{max} values. What mechanism this is could not be determined during the present research. Possibilities include void formation that is not in line with the main crack (and therefore does not contribute to crack advance), or secondary crack formation that was not visible from the side of the specimen. Further research is required to investigate these possibilities.

The numerical results confirm that increasing the adhesive thickness yields no substantial difference in the strain energy release rate. Considering the thickness-independent correlation between G_{max} and G^* shown in Fig. 11, this means that the resistance to crack growth is also independent of the thickness.

Conversely, more plastic dissipation was found in specimens with thicker adhesive. Comparing this with experimental results shows that the increased plasticity has a favourable effect on crack growth.

It seems likely that plastic deformation is related to some form of damage (e.g. voids) that contributes to crack growth. A recent investigation [46] using in-situ SEM observations of crack growth tests on CFRP suggests that, even under mode I loading, crack growth occurs by link-up of micro-cracks nucleating ahead of the crack tip. If plastic deformation prompted the formation of micro-cracks around the crack tip, that would explain why more crack growth was observed with thicker adhesive. In other words, in this case the plasticity around the crack tip has an anti-shielding effect.

The plasticity effect may also explain why secondary cracks developed in the thick specimens only in the first part of the test. From Fig. 16 we can see that most plasticity is produced when the applied U_{cyc} is high, i.e. at the beginning of the test, possibly resulting in micro-cracks formed at the sides of the crack tip, which link up creating secondary cracks. The formation of secondary cracks would then stop when the plastic deformation decreases under a certain level. Further investigations of the micro-mechanics of fatigue crack growth are required to test this hypothesis.

In terms of $\mathrm{d}U/\mathrm{d}a$ and $\mathrm{d}U/\mathrm{d}N$ the combination of the experimental and numerical results suggests the following: for a given load cycle (i.e. G_{max} and G_{min}), the amount of energy required per unit of crack growth, $\mathrm{d}U/\mathrm{d}a$, is not affected by the thickness. However, the increased plasticity for increased thickness allows more energy dissipation, $\mathrm{d}U/\mathrm{d}N$, in one cycle. This increased energy dissipation at the same $\mathrm{d}U/\mathrm{d}a$ results in an increased crack growth rate for a higher adhesive thickness.

The effect of increasing the thickness is opposite to most of the fatigue results from literature discussed above, including e.g. the results of Azari et al. [11], Mall and Ramamurthy [16] and Chai [13]. In fact, the damaging mechanism associated to plasticity would be obviously material dependent, and furthermore the thicknesses investigated here were lower than those used in previous studies, which could explain why opposite results are reported in the literature, i.e. a decreased crack growth rate with increasing adhesive thickness.

This suggests that also in fatigue there is an optimum thickness, such as found by Kinloch and Shaw [6] and Yan et al. [10] for the (quasi-static) fracture toughness. In the quasi-static case increasing the thickness above this optimum results in a lower fracture toughness; similarly, in fatigue it might result in a higher crack growth rate for a given load cycle. Kinloch and Shaw [6], and Bascom and Cottington [7] suggest that the highest G_c value is obtained when the plastic zone size at the critical load is equal to the adhesive thickness. Since the plastic zone size depends on the yield strength, this would make the optimum thickness material dependant.

Thus, a hypothesis can be formulated that could explain the difference between the present results and those reported in literature. That is that for the material tested here (FM94 epoxy), the optimum thickness is lower than the thicknesses tested, whereas

for results reported in literature the optimum thickness was higher than the thicknesses tested.

This hypothesis will have to be investigated in future research work, but it might for example explain the effect of thickness on the fracture toughness of PEEK reported by Chai [13].

9. Conclusions

A combination of experiments and numerical calculations was used to investigate the effect of adhesive thickness on fatigue crack growth in an FM94 epoxy adhesive bond.

For the range of thicknesses investigated in this research, increasing the adhesive thickness resulted in an increase of the crack growth rate. The resistance to crack growth (energy dissipation per unit crack growth) was not affected by changes in the adhesive thickness. However, the amount of energy available per unit crack growth, for a given load, increased when the adhesive thickness was increased. The net result was an increased growth rate.

The numerical results confirm that the resistance to crack growth is not affected by the adhesive thickness, although more plastic dissipation is found in thicker specimens. It is hypothesised that this plastic deformation allows more energy to be dissipated and promotes the formation of micro-cracks around the crack tip, which result in increased crack growth and creation of secondary cracks in thicker adhesives.

A more detailed investigation of the micro-mechanics of crack growth and the crack opening is needed in order to determine how exactly the plastic deformation influences the crack growth rate. Such an investigation may also be able to show if and when increased plastic dissipation leads to a shielding effect, reducing the crack growth rate, as has been reported in literature for larger adhesive thicknesses.

Furthermore, the present results show that the effect of adhesive thickness most likely depends on whether the thickness is smaller or greater than a material-dependant optimum thickness. Care must therefore be taken when assuming that trends observed in one adhesive will also apply to a different adhesive.

Declaration of Competing Interest

The authors declare that they have no known competing financial interests or personal relationships that could have appeared to influence the work reported in this paper.

Acknowledgements

J.A. Pascoe gratefully acknowledges the support of the Netherlands Organisation for Scientific Research in the form of a Mosaic grant, under project number: 017.009.005.

Appendix A. Supplementary material

Supplementary data associated with this article can be found, in the online version, at https://doi.org/10.1016/j.engfracmech.2020.106959.

References

[1] Pascoe JA, Alderliesten RC, Benedictus R. Methods for the prediction of fatigue delamination growth in composites and adhesive bonds - A critical review. Eng Fract Mech 2013;112–113:72–96. https://doi.org/10.1016/j.engfracmech.2013.10.003.
[2] Pascoe JA, Alderliesten RC, Benedictus R. On the physical interpretation of the R-ratio effect and the LEFM parameters used for fatigue crack growth in adhesive bonds. Int J Fatigue 2017;97. https://doi.org/10.1016/j.ijfatigue.2016.12.033.
[3] Pascoe JA, Alderliesten RC, Benedictus R. On the relationship between disbond growth and the release of strain energy. Eng Fract Mech 2015;133:1–13. https://doi.org/10.1016/j.engfracmech.2014.10.027.
[4] Alderliesten RC. How proper similitude can improve our understanding of crack closure and plasticity in fatigue. Int J Fatigue 2016;82:263–73. https://doi.org/10.1016/j.ijfatigue.2015.04.011.
[5] Pascoe J.A. Damage Tolerance of Adhesive Bonds – Datasets; 2014. https://doi.org/10.4121/uuid:c43549b8-606e-4540-b75e-235b1e29f81d.
[6] Kinloch AJ, Shaw SJ. The fracture resistance of a toughened epoxy adhesive. J Adhes 1981;12(1):59–77. https://doi.org/10.1080/00218468108071189.
[7] Bascom WD, Cottington RL, Jones RL, Peyser P. The fracture of epoxy- and elastomer-modified epoxy polymers in bulk and as adhesives. J Appl Polym Sci 1975;19(9):2545–62. https://doi.org/10.1002/app.1975.070190917.
[8] Wang SS, Mandell JF, McGarry FJ. An analysis of the crack tip stress field in DCB adhesive fracture specimens. Int J Fract 1978;14(1):39–58. https://doi.org/10.1007/BF00032383.
[9] Daghyani HR, Ye L, Mai YW. Mode-I fracture behaviour of adhesive joints. Part II. Stress analysis and constraint parameters. J Adhes 1995;53(3–4):163–72. https://doi.org/10.1080/00218469508009936.
[10] Yan C, Mai YW, Ye L. Effect of bond thickness on fracture behaviour in adhesive joints. J Adhes 2001;75(1):27–44. https://doi.org/10.1080/00218460108029592.
[11] Azari S, Papini M, Spelt JK. Effect of adhesive thickness on fatigue and fracture of toughened epoxy joints – Part I: Experiments. Eng Fract Mech 2011;78(1):153–62. https://doi.org/10.1016/j.engfracmech.2010.06.025.
[12] Azari S, Papini M, Spelt JK. Effect of adhesive thickness on fatigue and fracture of toughened epoxy joints – Part II: Analysis and finite element modeling. Eng Fract Mech 2011;78(1):138–52. https://doi.org/10.1016/j.engfracmech.2010.07.006.
[13] Chai H. On the correlation between the mode I failure of adhesive joints and laminated composites. Eng Fract Mech 1986;24(3):413–31. https://doi.org/10.1016/0013-7944(86)90071-8.
[14] Krenk S, Jönsson J, Hansen LP. Fatigue analysis and testing of adhesive joints. Eng Fract Mech 1996;53(6):859–72. https://doi.org/10.1016/0013-7944(95)

00150-6.
[15] Abou-Hamda M, Megahed M, Hammouda M. Fatigue crack growth in double cantilever beam specimen with an adhesive layer. Eng Fract Mech 1998;60(5–6):605–14. https://doi.org/10.1016/S0013-7944(98)00018-6.
[16] Mall S, Ramamurthy G. Effect of bond thickness on fracture and fatigue strength of adhesively bonded composite joints. Int J Adhes Adhes 1989;9(1):33–7. https://doi.org/10.1016/0143-7496(89)90144-9.
[17] Xu XX, Crocombe AD, Smith PA. Fatigue crack growth rates in adhesive joints tested at different frequencies. J Adhes 1996;58(3–4):191–204. https://doi.org/10.1080/00218469608015200.
[18] Schmueser DW. A fracture mechanics approach to characterizing cyclic debonding of varied thickness adhesive joints to electroprimed steel surfaces. J Adhes 1991;36(1):1–23. https://doi.org/10.1080/00218469108026520.
[19] Joseph R, Bell JP, Mcevily AJ, Liang JL. Fatigue crack growth in epoxy/aluminum and epoxy/steel joints. J Adhes 1993;41(1–4):169–87. https://doi.org/10.1080/00218469308026561.
[20] Wilson GS. Fatigue Crack Growth Prediction for generalized fiber metal laminates and hybrid materials [Ph.D. thesis]. Delft University of Technology; 2013. https://doi.org/10.4233/uuid:8925fc2a-47e8-457a-960c-f86b5065fa60.
[21] Azari S, Ameli A, Papini M, Spelt JK. Analysis and design of adhesively bonded joints for fatigue and fracture loading: a fracture-mechanics approach. J Adhes Sci Technol 2013;27(15):1681–711. https://doi.org/10.1080/01694243.2012.748434.
[22] Pardoen T, Ferracin T, Landis CM, Delannay F. Constraint effects in adhesive joint fracture. J Mech Phys Solids 2005;53(9):1951–83. https://doi.org/10.1016/j.jmps.2005.04.009.
[23] Chiu WK, Jones R. A numerical study of adhesively bonded lap joints. Int J Adhes Adhes 1992;12:219–25. https://doi.org/10.1016/0143-7496(92)90057-3.
[24] Gleich DM, Van Tooren MJ, Beukers A. Analysis and evaluation of bondline thickness effects on failure load in adhesively bonded structures. J Adhes Sci Technol 2001;15(9):1091–101. https://doi.org/10.1163/156856101317035503.
[25] Gleich DM, Van Tooren MJ, Beukers A. A stress singularity approach to failure initiation in a bonded joint with varying bondline thickness. J Adhes Sci Technol 2001;15(10):1247–59. https://doi.org/10.1163/156856101317048734.
[26] Lenwari A, Thepchatri T, Santisukpotha P. A fracture-based criterion for debonding strength of adhesive-bonded double-strap steel joints. Eng J 2012;16(1):17–25. https://doi.org/10.4186/ej.2012.16.1.17.
[27] Pascoe JA. Characterisation of fatigue crack growth in adhesive bonds [Ph.D. thesis]. Delft University of Technology; 2016. https://doi.org/10.4233/uuid:ebbf552a-ce98-4ab6-b9cc-0b939e12ba8b.
[28] Andresen HW, Echtermeyer AT. Critical energy release rate for a CSM reinforced carbon fibre composite/steel bonding. Compos Part A: Appl Sci Manuf 2006;37(5):742–51. https://doi.org/10.1016/j.compositesa.2005.06.009.
[29] Bürger D. Mixed-mode fatigue disbond on metallic bonded joints [Ph.D. thesis]. Delft University of Technology; 2015. https://doi.org/10.4233/uuid:ec4dbcd6-052d-4009-bf9e-cdcbf4614174.
[30] Pascoe JA, Al Amery AMKH, Zavatta N. Effect of Bondline Thickness on Fatigue Crack Growth in FM94; 2016. https://doi.org/10.4121/UUID:1495C951-33E2-43AB-9F41-5ED3B57BA02F.
[31] Zavatta N. Influence of adhesive thickness on adhesively bonded joints under fatigue loading [MSc. thesis]. University of Bologna; 2015.
[32] ASTM Standard, D5528–01 (2007) Standard Test Method for Mode I Interlaminar Fracture Toughness of Unidirectional Fiber-Reinforced Polymer Matrix Composites; 2007. https://doi.org/10.1520/D5528-01R07E03.
[33] Pascoe J, Zavatta N, Alderliesten R, Benedictus R. Effect of Bondline Thickness on Fatigue Crack Growth in FM94 Epoxy Adhesive Bonds - Dataset 2; 2017. https://doi.org/10.4121/uuid:4400f37c-7168-4275-a778-09b237bd34c6.
[34] Rask M, Sørensen B. Determination of the J integral for laminated double cantilever beam specimens: The curvature approach. Eng Fract Mech 2012;96:37–48. https://doi.org/10.1016/j.engfracmech.2012.06.017.
[35] Goutianos S, Sørensen BF. Fracture resistance enhancement of layered structures by multiple cracks. Eng Fract Mech 2016;151:92–108. https://doi.org/10.1016/j.engfracmech.2015.10.036.
[36] Irwin G. Analysis of stresses and strains near the end of a crack traversing a plate. ASME J Appl Mech 1957;24:361–4.
[37] Irwin G, Kies J. Critical energy rate analysis of fracture strength. Weld J Res Suppl 1954;33:193s–8s.
[38] Pascoe JA, Alderliesten RC, Benedictus R. Characterising resistance to fatigue crack growth in adhesive bonds by measuring release of strain energy. In: Procedia structural integrity, Vol. 2; 2016. p. 80–7. https://doi.org/10.1016/j.prostr.2016.06.011.
[39] ASM Handbook Committee, ASM Handbook Volume 2: Properties and Selection: Nonferrous Alloys and Special-Purpose Materials, ASM International; 1990. https://doi.org/10.31399/asm.hb.v02.9781627081627.
[40] Cytec Engineered Materials, FM 94 Adhesive Film Technical Data Sheet; 2010.
[41] Papanicolaou GC, Charitidis P, Mouzakis DE, Karachalios E, Jiga G, Portan DV. Experimental and numerical investigation of balanced Boron/Epoxy single lap joints subjected to salt spray aging. Int J Adhes Adhes 2016;68:9–18. https://doi.org/10.1016/j.ijadhadh.2016.01.009.
[42] Rybicki EF, Kanninen MF. A finite element calculation of stress intensity factors by a modified crack closure integral. Eng Fract Mech 1977;9(4):931–8. https://doi.org/10.1016/0013-7944(77)90013-3.
[43] Krueger R. Virtual crack closure technique: history, approach, and applications. Appl Mech Rev 2004;57(1–6):109–43. https://doi.org/10.1115/1.1595677.
[44] Jokinen J, Wallin M, Saarela O. Applicability of VCCT in mode I loading of yielding adhesively bonded joints – a case study. Int J Adhes Adhes 2015;62:85–91. https://doi.org/10.1016/j.ijadhadh.2015.07.004.
[45] Amaral L, Yao L, Alderliesten R, Benedictus R. The relation between the strain energy release in fatigue and quasi-static crack growth. Eng Fract Mech 2015;145:86–97. https://doi.org/10.1016/j.engfracmech.2015.07.018.
[46] Khan R, Alderliesten R, Badshah S, Khattak MA, Khan MS, Benedictus R. Experimental investigation of the microscopic damage development at mode I fatigue delamination tips in carbon/epoxy laminates. Jurnal Teknologi 2016;78(11):33–40. https://doi.org/10.11113/.v78.8072.